Journal of Young Pharmacists, 2026; 18(3):917-930.
https://www.jyoungpharm.org

Original Article

Integrative Network Pharmacology and Molecular Docking Reveal the Multitarget Anti-HGSOC Potential of *Pterocarpus marsupium* Phytoconstituents via Modulation of HIF-1α-Driven Inflammation-Metabolism Crosstalk

Sambasivam Gopinath*, Pavithra Balakrishnan, Yamini Muli, Sabrin Sirajudeen, Pratheesha Vijaya Kumar Rajathi, Mohan Raj Vijayan

Department of Pharmacy Practice, Saveetha College of Pharmacy, SIMATS, Thandalam, Chennai, Tamil Nadu, INDIA.

ABSTRACT

Background: High-Grade Serous Ovarian Cancer (HGSOC) is the most lethal gynaecological malignancy, and its progression is driven substantially by Hypoxia-Inducible Factor-1α (HIF-1α)-centred inflammation-metabolism crosstalk that underlies chemoresistance. *Pterocarpus marsupium*, a plant used in Ayurvedic medicine for inflammatory and metabolic disorders, has not previously been investigated against HGSOC. **Purpose:** This study aimed to identify bioactive *P. marsupium* phytochemicals capable of multitarget modulation of the HIF-1α-driven hypoxia-inflammation-metabolism axis in HGSOC, using an integrated network pharmacology and molecular docking approach. **Materials and Methods:** Phytochemicals curated from the IMPPAT database were filtered using Lipinski's Rule of Five, SwissADME-predicted pharmacokinetics, and ProTox-3.0 toxicity screening. Putative human targets, predicted with SwissTargetPrediction, were intersected with HGSOC-associated genes from GeneCards and OMIM. A protein-protein interaction network was built in STRING/Cytoscape, and hub genes and functional modules were identified using cytoHubba and MCODE. Gene Ontology and KEGG pathway enrichment were performed in DAVID. Twenty-one drug-like phytochemicals were docked in triplicate, using CB-Dock, against five network-prioritised targets central to the hypoxia-glycolysis-survival axis - Factor Inhibiting HIF-1 (*FIH-1/HIF1AN*, a direct upstream regulator of HIF-1α transactivation), *PDK1*, *LDHA, MTOR*, and *STAT3* - and redocking of native co-crystallised ligands with RMSD analysis was performed to benchmark pose reliability. **Results:** Network analysis identified 107 shared targets and highlighted *HIF1A, IL6, EGFR, ESR1*, and *BCL2* as central regulatory hubs enriched in HIF-1, PI3K-Akt, and ErbB signalling pathways. Molecular docking showed that Pseudobaptigenin, 3,7,4′-trihydroxyflavone, and marsupsin achieved binding affinities of -8.3 to -9.7 kcal/mol across the panel, and redocking of native ligands reproduced experimental poses with RMSD values mostly below 2.0 Å, supporting the reliability of the docking protocol. **Conclusion:** These findings, supported by redocking/RMSD-validated binding poses, suggest that *P. marsupium* phytochemicals may act as multitarget modulators of the HGSOC hypoxia-inflammation-metabolism axis, offering a testable molecular rationale that bridges traditional Ayurvedic use with systems pharmacology. As this is an entirely computational study, these results are hypothesis-generating rather than confirmatory, and experimental validation is required before any therapeutic potential can be inferred.

Keywords: Ayurvedic medicine, HIF-1α signalling, High-grade serous ovarian cancer, Molecular docking, Network pharmacology, *Pterocarpus marsupium*.

Correspondence:
Dr. Sambasivam Gopinath
Associate Professor, Department of Pharmacy Practice, Saveetha College of Pharmacy, SIMATS, Thandalam, Chennai-602105, Tamil Nadu, INDIA.
Email: gopimbapharma@gmail.com
ORCID:0000-0003-2725-4863

Received: 03-06-2026;
Revised: 28-07-2026;
Accepted: 08-09-2026.

INTRODUCTION

High-Grade Serous Ovarian Carcinoma (HGSOC) remains the most lethal gynaecological malignancy, accounting for 70-80% of epithelial ovarian cancer deaths worldwide (Fu *et al*., 2025). Despite intensive therapeutic efforts, overall five-year survival has stalled near 49.1%, and patients with advanced-stage (III-IV) disease face a five-year survival rate below 25%, underscoring a persistent therapeutic impasse (Ahn *et al*., 2024). A key contributor to this poor outcome is late diagnosis: approximately 70-75% of patients present at stage III-IV, whereas five-year survival exceeds

DOI: 10.5530/jyp.20260099

Copyright Information :
Copyright Author (s) 2026 Distributed under Creative Commons CC-BY 4.0

Publishing Partner : Manuscript Technomedia. [www.mstechnomedia.com]

90% when the disease is detected early (Fu *et al.*, 2025). At the molecular level, HGSOC is characterised by near-universal TP53 mutation (~96% of cases) together with marked metabolic reprogramming, which together create formidable barriers to durable treatment response (Fu *et al.*, 2025).

Central to HGSOC aggressiveness is Hypoxia-Inducible Factor-1 alpha (HIF-1α), a master transcriptional regulator that orchestrates convergence of the inflammatory and metabolic pathways driving disease progression (Rahman *et al.*, 2025). Under the hypoxic conditions pervasive in solid tumours, stabilised HIF-1α activates over 100 target genes, driving glycolytic enzyme upregulation (HK2, LDHA, PDK1) and proinflammatory cytokine release (IL-6, TNF-α, CXCL8) (Rahman *et al.*, 2025; Shaikat *et al.*, 2025; Wang X *et al.*, 2021). This inflammation-metabolism crosstalk forms a self-amplifying loop that promotes chemoresistance through enhanced drug-efflux transporter expression, suppressed apoptotic signalling, and upregulated cancer stem cell markers (CD133, ALDH, OCT4) associated with treatment failure and metastasis (Fu *et al.*, 2025; Wagner *et al.*, 2025). HIF-1α additionally induces VEGF and epithelial-mesenchymal transition, facilitating angiogenesis and dissemination (Rahman *et al.*, 2025). Although first-line platinum-based chemotherapy achieves an initial response in roughly 80% of patients, more than 70% subsequently develop platinum-resistant recurrence within 12-24 months, with a median survival thereafter of only 7-12 months, highlighting the need for multitarget therapeutic strategies (Qin *et al.*, 2017).

Current single-target agents fail to address the integrated HIF-1α-driven network underlying HGSOC progression. Conventional cytotoxic chemotherapy damages rapidly dividing cells but cannot suppress the adaptive HIF-1α-mediated responses that sustain resistance (Fu *et al.*, 2025), while the hypoxic microenvironment itself limits drug penetration and fosters an immunosuppressive stroma (Fu *et al.*, 2025). No currently available agent effectively suppresses the interconnected inflammation-metabolism networks that drive this malignancy, leaving a substantial therapeutic gap that motivates the search for multitarget natural-product leads.

Pterocarpus marsupium Roxb. (Indian kino tree), a staple of Ayurvedic medicine for metabolic and inflammatory disorders, is rich in bioactive phytoconstituents with multimodal pharmacological potential, including pterostilbene - a dimethylated resveratrol analogue with high oral bioavailability (80-95%) - alongside epicatechin, marsupsin, liquiritigenin, and other polyphenols (Liu *et al.*, 2024). Pterostilbene exhibits anti-inflammatory activity through NF-κB inhibition and antioxidant activity via Nrf2 pathway activation, and has been shown to modulate the MTA1/HIF-1α axis, suppressing proliferation and angiogenesis in murine models (Liu *et al.*, 2024). This mechanistic link to HIF-1α-dependent pathology, together with emerging evidence that natural products targeting cancer stem cell populations can re-sensitise resistant tumours to conventional therapy (Opara *et al.*, 2025), suggested that *P. marsupium* constituents merited systematic investigation against HGSOC - an association that, to our knowledge, has not previously been examined.

Network pharmacology offers a systems-level paradigm for identifying multitarget therapeutic effects from multicomponent natural products (Zhang *et al.*, 2013), and when coupled with molecular docking and pathway enrichment analysis, it enables a mechanistic account of how phytochemicals may coordinate action across interconnected disease nodes - precisely the strategy required to address the adaptive complexity of HGSOC. This study therefore aimed to: (i) identify and characterise bioactive *P. marsupium* constituents and their putative molecular targets; (ii) construct compound-target-pathway networks describing multitarget effects on HIF-1α signalling, glycolysis, inflammation, and angiogenesis; (iii) perform molecular docking of prioritised phytoconstituents against key regulatory hubs of the hypoxia-metabolism axis; and (iv) perform pathway enrichment analysis to propose plausible anti-HGSOC mechanisms. By linking traditional ethnopharmacological knowledge with contemporary systems pharmacology, this work is intended to generate a testable molecular hypothesis - rather than a confirmed therapeutic claim - to guide future experimental validation of multitarget chemosensitising strategies for HGSOC.

MATERIALS AND METHODS

Phytochemical Dataset and Ethnopharmacological Rationale

The phytochemical dataset was derived from the heartwood and kino gum of P. marsupium, plant parts with a documented history in Ayurvedic medicine for the management of diabetes and inflammatory disorders (Vivek-Ananth *et al.*, 2023; Warrier *et al.*, 1994). Bioactive compounds, including PubChem CIDs, IUPAC names, SMILES strings, and 3D SDF structures, were retrieved from the Indian Medicinal Plants, Phytochemistry and Therapeutics (IMPPAT) database, a curated, peer-reviewed repository specific to Indian medicinal flora; this database was selected over generic chemical repositories because it provides ethnopharmacologically annotated, plant-part-specific constituent lists, reducing the risk of including compounds not actually present in the plant material of interest. Cross-referencing against PubChem and ChemSpider was performed to eliminate duplicate entries and verify structural integrity prior to downstream screening.

Drug-Likeness, Pharmacokinetic, and Toxicity Screening

Physicochemical properties were evaluated against Lipinski's "Rule of Five" (Lipinski *et al.*, 2001), and ADMET profiles were predicted using SwissADME (Daina *et al.*, 2017). Toxicity

assessment was performed using ProTox-3.0 to exclude compounds with predicted mutagenicity or high acute toxicity (Banerjee *et al.*, 2018; Kim *et al.*, 2022). Lipinski, SwissADME, and ProTox were selected because they are among the most extensively validated, freely accessible platforms for early-stage drug-likeness triage and are widely adopted in network pharmacology workflows, allowing direct comparability with prior phytochemical studies. Compounds violating more than one Lipinski criterion, or flagged as high-probability mutagens/hepatotoxicants by ProTox-3.0, were excluded from further analysis.

Target Prediction and Disease Gene Mapping

Putative human protein targets of the shortlisted phytochemicals were predicted using SwissTargetPrediction, which combines 2D and 3D chemical similarity against a curated bioactive ligand library (Daina *et al.*, 2019; Berman H *et al.*, 2014). Only targets returned as high-confidence predictions for the Homo sapiens taxonomic filter were retained; compounds returning no high-confidence human target were excluded from network construction. [Authors: please state and cite the exact SwissTargetPrediction probability-score cut-off applied (e.g., Probability > 0), as this numeric threshold was not specified in the original submission and reviewers will expect the precise value.] HGSOC-associated disease genes were compiled from GeneCards (v2.1.16) (GeneCards, 2017) and OMIM® (Hamosh *et al.*, 2005), two complementary, manually curated gene-disease databases chosen to maximise coverage of both well-established and recently reported HGSOC-relevant genes. The predicted target set was intersected with the disease gene set using Venny 2.1 (Oliveros, 2007) to yield the common, disease-relevant therapeutic interface analysed in subsequent network steps.

Functional Enrichment Analysis

Gene Ontology (molecular function, biological process, cellular component) and KEGG pathway enrichment of the shared targets were performed using DAVID, with terms considered significantly enriched at $p<0.05$ (Sherman *et al.*, 2024; Kanehisa, 2000; Kanehisa and Goto, 2000; Kanehisa *et al.*, 2025). DAVID was selected as one of the most extensively benchmarked functional annotation platforms for translating target lists into mechanistic pathway hypotheses, facilitating comparison with the existing network pharmacology literature.

Protein-Protein Interaction Network Construction and Hub Gene Prioritisation

The common target genes were submitted to STRING (minimum required interaction confidence score ≥ 0.700, STRING's "high confidence" tier) to construct a Protein-Protein Interaction (PPI) network, visualised and analysed in Cytoscape 3.10.3 (Szklarczyk *et al.*, 2023; Franz *et al.*, 2023). This threshold was chosen to minimise false-positive interactions while retaining sufficient network density for topological analysis. The MCODE plugin was used to identify densely connected functional modules, retaining clusters with an MCODE score > 2 (Bader and Hogue, 2003); cytoHubba was used to rank nodes by degree centrality (Chin *et al.*, 2014). Hub genes were operationally defined as nodes occupying the highest degree-centrality tier of the network (connectivity degree ≥ 94, the top decile of connected nodes); this data-driven threshold was applied uniformly, and the biological plausibility of each resulting hub was cross-checked against its literature-reported role in hypoxia, inflammation, or metabolic signalling before being carried forward for pathway interpretation.

Network Integration and Gene-Disease Mapping

A bipartite compound-target network linking priority phytochemicals to their predicted targets was constructed in Cytoscape, with edge weights reflecting target-prediction confidence. Hub genes were additionally mapped to associated disorders using MalaCards to contextualise their broader pathological relevance and support the biological plausibility of *P. marsupium* as a multitarget modulator (Rappaport *et al.*, 2017).

Target Selection and Structural Basis for Docking

Candidate docking targets were shortlisted using a pre-specified, multi-tiered rationale combining (i) topological centrality (degree and MCODE cluster membership) within the PPI network, (ii) enrichment-derived pathway relevance to the HIF-1 signalling and metabolic reprogramming axes identified in Section 2.4, and (iii) independent mechanistic relevance to HGSOC chemoresistance reported in the literature. Based on these criteria, five key proteins representing the hypoxia-glycolysis-survival axis were selected: FIH-1 (HIF1AN), PDK1, LDHA, MTOR, and STAT3. FIH-1 (Factor Inhibiting HIF-1; PDB: 7A1J) is a 2-oxoglutarate/Fe (II)-dependent asparaginyl hydroxylase that regulates HIF-1α transcriptional activity by hydroxylating its C-terminal transactivation domain, thereby preventing CBP/p300 co-activator recruitment (Lando *et al.*, 2002). As a direct regulator of the HIF-1 signalling axis identified in the network analysis, FIH-1 was selected to represent this pathway. The remaining targets included PDK1 (PDB: 1OKZ), a key regulator of pyruvate metabolism; LDHA (PDB: 6Q0D), a critical glycolytic enzyme; MTOR (PDB: 4JSX), a master regulator of cell growth and metabolism; and STAT3 (PDB: 6NJS), an important mediator of cytokine signalling and tumour progression. All five crystal structures were selected based on high structural resolution and the availability of co-crystallized ligands, enabling accurate definition of the native binding pockets. Active-site residues were identified from the co-crystallized complexes using PDBsum (Table 1) (Laskowski *et al.*, 2018), ensuring that molecular docking was performed within experimentally validated functional binding sites.

Molecular Docking Protocol

Cavity-detecting, blind molecular docking was performed using CB-Dock, which identifies candidate binding cavities directly from receptor surface curvature before docking, reducing operator-introduced bias in pocket selection relative to manually defined grid boxes (Liu *et al.*, 2022). Binding affinities (ΔG, kcal/mol) were calculated for all 21 drug-like phytochemicals against each of the five prioritised targets, with more negative values indicating stronger predicted binding. Post-docking interaction analysis was performed in Discovery Studio Visualiser to characterise non-covalent contacts, including hydrogen bonds, hydrophobic interactions, and π-π stacking (Dassault Systèmes, 2016).

Docking Validation: Redocking and RMSD Analysis

Three validation measures were incorporated into the docking workflow. First, docking pockets were anchored to the empirically defined, co-crystallised ligand-binding sites of each receptor (Table 1) rather than to computationally predicted pockets, constraining predicted poses to biologically relevant cavities. Second, all 105 compound-target combinations (21 phytochemicals × 5 targets) were docked in technical triplicate (independent CB-Dock runs, denoted T1-T3 in Table 2) to assess the reproducibility of the predicted binding affinities; the coefficient of variation across replicates was low (≤ 0.1 kcal/mol for the large majority of compound-target pairs), indicating stable scoring under the docking protocol used. Third, redocking of the native co-crystallised ligand into its own empirically defined pocket was performed as part of the standard docking protocol for all 105 compound-target complexes; RMSD benchmarking against the experimental crystallographic pose, using Discovery Studio Visualiser (Superimpose Structures protocol) to calculate heavy-atom root-mean-square deviation, was then carried out for the highest-affinity complexes identified across the full panel (Table 3), representing the leads of greatest mechanistic interest. Conventionally, RMSD<2.0 Å is taken as evidence of correct pose reproduction by the docking protocol.

RESULTS

Phytochemical Screening and Pharmacokinetic Profiling

Of the 30 bioactive phytoconstituents catalogued for *P. marsupium*, 21 (70%) satisfied the drug-likeness and pharmacokinetic criteria and were carried forward for network analysis. Of these, 61.9% fully complied with Lipinski's Rule of Five, and the remaining 38.1% showed only a single, minor violation. The mean molecular weight of the selected library was 269.69±72.19 Da, and the mean topological polar surface area was 56.20±28.34 Å², both within ranges favourable for cellular permeability (≤140 Å²). Predicted gastrointestinal absorption was high for 81.0% of compounds, with a mean bioavailability score of 0.650±0.145, low mean hydrogen-bond donor count (1.95±1.20), and low mean acceptor count (3.10±1.61). The final library spanned three pharmacologically distinct chemical classes - phenolics (*n*=10), saturated fatty acids (*n*=6), and terpenoids (*n*=5) - and predictive toxicology did not flag major mutagenicity, carcinogenicity, or hERG-inhibition liability for any retained compound, supporting their suitability for downstream *in silico* modelling.

Table 1: Active-Site Residues of Target Functional Sites, Defined from Co-Crystallised Ligand Complexes.

Target Gene	Protein (Receptor/ Transporter)	PDB ID	Standard Ligand	Active Site Residues
HIF1AN	Factor Inhibiting HIF-1 (FIH-1)	7A1J	QVN - 3-(3-Phenylpropyl) -2-Oxoglutarate	102:A,145:A,147:A,188:A,196:A,199:A,201:A,205:A,207:A, 214:A,239:A,279:A,281:A,294:A,296:A,401:A,407:A
PDK1	Pyruvate Dehydrogenase Kinase 1	1OKZ	UCN-01 (7-Hydroxystaurosporine)	88:A,212:A,96:A,223:A,109:A,161:A,165:A,89:A,111:A,159 :A,210:A,143:A,1370:A,222:A,162:A,166:A,209:A,160:A
LDHA	Lactate Dehydrogenase A	6Q0D	Pyrazole-based LDHA inhibitor (NCGC00384414-01)	138:A,137:A,238:A,105:A,164:A,193:A,237:A,241:A,108:A, 194:A,322:A,325:A,192:A,140:A,168:A,141:A,191:A,247:A ,165:A,139:A
MTOR	Mammalian Target of Rapamycin	4JSX	Torin2 (ATP-competitive mTOR kinase inhibitor)	2239: B, 2345: B, 2356: B, 2237: B, 2243: B, 2185: B, 2238: B, 2245: B, 2342: B, 2601: B, 2240: B
STAT3	Signal Transducer and Activator of Transcription 3	6NJS	SD-36 (STAT3 selective degrader/inhibitor)	637:A, 639:A, 640:A,658613:A, 611:A, 612:A, 644:A:A, 659:A, 666:A, 701:A,638:A, 609:A, 636:A, 657:A,

Notes: Active-site residues were identified directly from the co-crystallised PDB complexes using PDBsum, ensuring an empirically defined docking grid (Section 2.7).

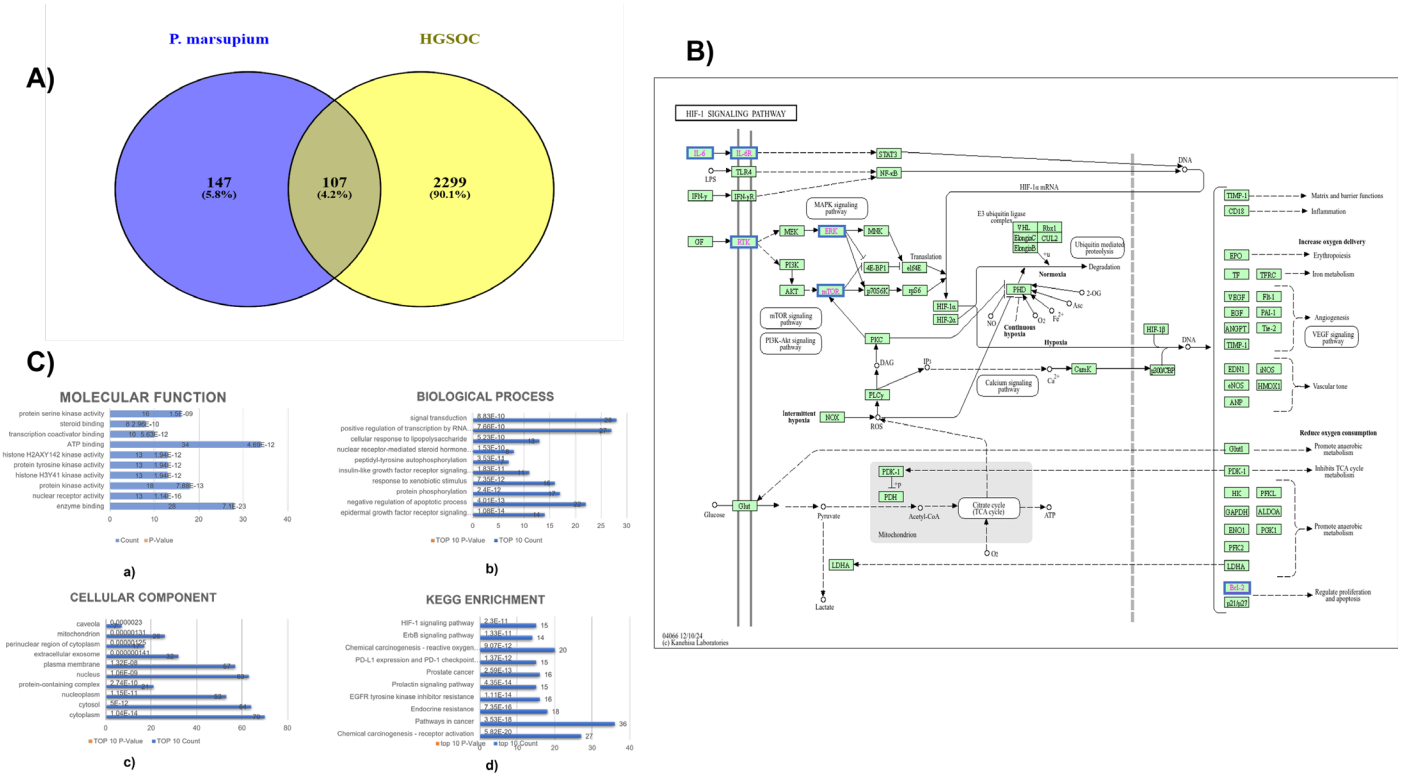


Figure 1: Systems pharmacology mapping and functional enrichment analysis of *P. marsupium* against HGSOC. (A) Venn diagram of the target intersection between *P. marsupium* bioactive constituents (blue) and HGSOC-associated genes (yellow), identifying 107 common therapeutic targets. (B) KEGG map of the HIF-1 signalling pathway, highlighting regulatory nodes targeted by the phytochemicals. (C) Functional annotation profiling: (a) GO Molecular Function; (b) GO Biological Process; (c) GO Cellular Component; (d) Top 10 enriched KEGG pathways.

Target Prediction and Disease Mapping

SwissTargetPrediction returned 308 independent protein targets and 737 compound-target interactions across the 21-compound library, with a target density of 19-100 targets per molecule (median 45), indicating substantial multitarget potential. Thirteen structurally distinct, comparatively under-explored constituents - including gallic acid, pterostilbene, and several saturated fatty acids - were prioritised for closer mechanistic interpretation based on this multitarget profile and their limited prior investigation in HGSOC. Mapping the predicted target set against HGSOC-relevant genes (GeneCards and OMIM) identified 107 overlapping targets, corresponding to 42.1% of all predicted phytochemical targets (Figure 1A). Functional categorisation of these shared targets revealed a regulatory landscape spanning enzymes, nuclear receptors, kinases, and G-protein-coupled receptors, consistent with a plausible multitarget mechanism for *P. marsupium* activity in HGSOC-relevant pathways.

Functional Enrichment and Pathway Prioritisation

Gene Ontology enrichment of the 107 shared targets showed significant overrepresentation of protein serine kinase activity, ATP binding, and nuclear receptor activity (molecular function; Figure 1Ca); signal transduction, apoptotic regulation, and hypoxic-stimulus response (biological process; Figure 1Cb); and target engagement at membrane and cytoplasmic compartments (cellular component; Figure 1Cc). KEGG pathway analysis identified significant enrichment of the HIF-1, ErbB, and PD-L1/PD-1 immune checkpoint signalling pathways (Figure Cd), together with the PI3K-Akt and mTOR pathways directly implicated in HGSOC chemoresistance. Mapping of hub genes onto the HIF-1 signalling cascade positioned *STAT3, IL6, NFκB, AKT, MTOR*, and *BCL2* as key regulatory nodes linking upstream inflammatory cytokine signalling to downstream metabolic reprogramming and survival signalling (Figure 1B), supporting a pathway-centric rationale for the subsequent choice of docking targets.

Protein-Protein Interaction Network and Cluster Analysis

The STRING-derived PPI network of the 107 shared targets (confidence ≥ 0.700) comprised 107 nodes and 1,085 edges (Figure 2A). Topological analysis identified *EGFR, IL6, ESR1, CTNNB1, BCL2, SRC, MAPK3, PPARG, PTGS2*, and *MTOR* as high-degree hub proteins (degree range 94-146), consistent with a role as master regulators bridging oncogenic, metabolic, and inflammatory signalling in HGSOC (Figure 2C). MCODE analysis resolved five functional modules (Figure 2B): Cluster 1 (35 nodes, 882 edges; MCODE score 25.9), the principal regulatory core, encompassed PI3K/AKT/mTOR, HIF-1, and NF-κB pathway mediators; Cluster 2 comprised nuclear receptors and metabolic regulators (*RXRA, RARA, PPARD*); Cluster 3 comprised the

drug-metabolising enzymes *CYP3A4* and *CYP1B1*; and Clusters 4 and 5 were associated with DNA-repair and mitogenic-signalling components, respectively. This modular architecture indicates that *P. marsupium* constituents likely engage an integrated network of tumour-survival pathways rather than isolated single proteins.

Compound-Target and Gene-Disease Integration

The bipartite compound-target network, comprising 13 priority phytochemicals mapped to 308 predicted targets (321 nodes, 737 edges), identified pterostilbene (100 targets), linoleic acid (94 targets), and oleic acid (88 targets) as the principal multitarget hubs (Figure 3A), with high-confidence associations to cytochrome P450 19A1, androgen receptor, and carbonic anhydrase II. Gene-disease mapping of hub genes via MalaCards placed *EGFR, IL6, ESR1, CTNNB1, BCL2, SRC*, and *PPARG* at dense points of connectivity spanning breast and colorectal cancer alongside comorbid inflammatory and metabolic disorders (Figure 3B), consistent with broad translational relevance for *P. marsupium* constituents as multitarget modulators, while underscoring that the present evidence remains associative and computational rather than causal.

Molecular Docking and Structural Interaction Analysis

All 21 drug-like phytochemicals were docked in technical triplicate against the five network-prioritised targets (FIH-1/*HIF1AN, PDK1, LDHA, MTOR, STAT3*; Figure 4A; full triplicate results in Table 2). Replicate binding affinities were highly consistent (inter-run spread typically ≤ 0.1-0.2 kcal/mol), supporting the reproducibility of the docking protocol. Pseudobaptigenin and 3,7,4′-trihydroxyflavone were the strongest overall binders, with mean binding energies of -9.7 kcal/mol at FIH-1 (Table 2). *LDHA* was most strongly engaged by oleanolic acid (-8.6 kcal/mol) and *PDK1* by Naringetol/Pseudobaptigenin (-8.6 kcal/mol), while *MTOR* affinity peaked at -8.8 kcal/mol (Pseudobaptigenin), and, following data verification, *STAT3* was likewise most strongly engaged by Pseudobaptigenin (-8.8 kcal/mol; Naringetol at *STAT3* was re-verified at -6.4 kcal/mol, correcting the -8.5 kcal/mol value flagged as a probable data-entry duplication

Table 2: Binding Affinities of Lead Phytochemicals at Network-Prioritised HGSOC Targets.

Sl. No.	Target	Ligands	Pubchem ID	Binding Affinity (kcal/mol)			Binding Affinity (kcal/mol)
				T1	T2	T3	
1.	FIH-1 (HIF1AN)	Gallic acid	370	-6.6	-6.6	-6.7	-6.6
2.		Pterostilbene	5281727	-7.5	-7.4	-7.5	-7.5
3.		4-[2-Hydroxy-3-(4-hydroxyphenyl) propyl] phenol	185124	-9.1	-9.2	-9.1	-9.1
4.		Ebanol	6437266	-6.6	-6.7	-6.6	-6.6
5.		4-Hydroxybenzaldehyde	126	-5.6	-5.6	-5.7	-5.6
6.		beta-Eudesmol	91457	-7.1	-7.1	-7.2	-7.1
7.		Myristic acid	11005	-5.7	-5.7	-5.5	-5.7
8.		Palmitic acid	985	-5.8	-5.8	-5.8	-5.8
9.		Oleic acid	445639	-.6.8	-6.7	-6.8	-6.8
10.		Linoleic acid	5280450	-6.8	-6.8	-6.9	-6.8
11.		Abscisic Acid	5280896	-6.9	-6.7	-6.9	-6.9
12.		Marsupsin	134369	-9.3	-9.3	-9.4	-9.3
13.		Epicatechin	72276	-8.3	-8.3	-8.3	-8.3
14.		Bergenin	66065	-6.8	-6.8	-6.7	-6.8
15.		liquiritigenin	114829	-8.9	-8.9	-8.8	-8.9
16.		Isoliquiritigenin	638278	-7.9	-7.9	-7.8	-7.9
17.		Naringetol	439246	-9.2	-9.2	-9.3	-9.2
18.		Pseudobaptigenin	5281805	-9.7	-9.7	-9.8	-9.7
19.		3,7,4'-Trihydroxyflavone	5281611	-9.7	-9.7	-9.7	-9.7
20.		Lupeol	259846	-8.4	-8.4	-8.5	-8.4
21.		Oleanolic acid	10494	-8.3	-8.4	-8.3	-8.3

22.	PDK1	Gallic acid	370	-5.5	-5.4	-5.5	-5.5
23		Pterostilbene	5281727	-7.4	-7.5	-7.4	-7.4
24.		4-[2-Hydroxy-3-(4-hydroxyphenyl) propyl] phenol	185124	-7.7	-7.6	-7.7	-7.7
25.		Ebanol	6437266	-6.2	-6.3	-6.2	-6.2
26.		4-Hydroxybenzaldehyde	126	-5.1	-5.2	-5.1	-5.1
27.		beta-Eudesmol	91457	-7.1	-7.2	-7.1	-7.1
28.		Myristic acid	11005	-5.4	-5.4	-5.5	-5.4
29.		Palmitic acid	985	-5.4	-5.4	-5.4	-5.4
30.		Oleic acid	445639	-5.6	-5.6	-5.6	-5.6
31.		Linoleic acid	5280450	-6	-6	-6	-6
32.		Abscisic Acid	5280896	-7.1	-7.1	-7.2	-7.1
33.		Marsupsin	134369	-8.3	-8.3	-8.4	-8.3
34.		Epicatechin	72276	-8.1	-8.1	-8.2	-8.1
35.		Bergenin	66065	-7.8	-7.8	-7.9	-7.8
36.		liquiritigenin	114829	-8.4	-8.5	-8.4	-8.4
37.		Isoliquiritigenin	638278	-7.6	-7.7	-7.6	-7.6
38.		Naringetol	439246	-8.6	-8.8	-8.6	-8.6
39.		Pseudobaptigenin	5281805	-8.6	-8.6	-8.8	-8.6
40.		3,7,4'-Trihydroxyflavone	5281611	-7.9	-7.9	-7.9	-7.9
41.		Lupeol	259846	-7.6	-7.6	-7.7	-7.6
42.		Oleanolic acid	10494	-8.2	-8.2	-8.3	-8.2
43.	LDHA	Gallic acid	370	-5.6	-5.5	-5.6	-5.6
44.		Pterostilbene	5281727	-7.1	-7.2	-7.1	-7.1
45.		4-[2-Hydroxy-3-(4-hydroxyphenyl) propyl] phenol	185124	-7.2	-7.3	-7.2	-7.2
46.		Ebanol	6437266	-5.5	-5.5	-5.5	-5.5
47.		4-Hydroxybenzaldehyde	126	-5.2	-5.2	-5.3	-5.2
48.		beta-Eudesmol	91457	-6.3	-6.3	-6.4	-6.3
49.		Myristic acid	11005	-4.8	-4.8	-4.9	-4.8
50.		Palmitic acid	985	-5.3	-5.3	-5.4	-5.3
51.		Oleic acid	445639	-4.6	-4.6	-4.7	-4.6
52.		Linoleic acid	5280450	-5.5	-5.5	-5.5	-5.5
53.		Abscisic Acid	5280896	-6.4	-6.4	-6.5	-6.4
54.		Marsupsin	134369	-7.2	-7.2	-7.3	-7.2
55.		Epicatechin	72276	-7.4	-7.5	-7.4	-7.4
56.		Bergenin	66065	-7.8	-7.9	-7.8	-7.8
57.		liquiritigenin	114829	-7.6	-7.6	-7.6	-7.6
58.		Isoliquiritigenin	638278	-6.8	-6.8	-6.8	-6.8
59.		Naringetol	439246	-7.3	-7.3	-7.3	-7.3
60.		Pseudobaptigenin	5281805	-7.5	-7.4	-7.5	-7.5
61.		3,7,4'-Trihydroxyflavone	5281611	-7.5	-7.6	-7.5	-7.5
62.		Lupeol	259846	-8.1	-8.2	-8.1	-8.1
63.		Oleanolic acid	10494	-8.6	-8.5	-8.6	-8.6

64.	MTOR	Gallic acid	370	-5.3	-5.4	-5.3	-5.3
65.		Pterostilbene	5281727	-7.6	-7.6	7.7	-7.6
66.		4-[2-Hydroxy-3-(4-hydroxyphenyl) propyl] phenol	185124	-7.8	-7.8	7.8	-7.8
67.		Ebanol	6437266	-6.8	-6.8	-6.9	-6.8
68.		4-Hydroxybenzaldehyde	126	-4.9	-4.9	-4.8	-4.9
69.		beta-Eudesmol	91457	-7.4	-7.4	-7.5	-7.4
70.		Myristic acid	11005	-5	-5	-5.1	-5
71.		Palmitic acid	985	-5.5	-5.5	-5.4	-5.5
72.		Oleic acid	445639	-4.9	-4.9	-5	-4.9
73.		Linoleic acid	5280450	-5.8	-5.9	-5.8	-5.8
74.		Abscisic Acid	5280896	-6.4	-6.5	-6.4	-6.4
75.		Marsupsin	134369	-7.2	-7.3	-7.2	-7.2
76.		Epicatechin	72276	-7.9	-8	-7.9	-7.9
77.		Bergenin	66065	-6.5	-6.5	-6.5	-6.5
78.		liquiritigenin	114829	-8.5	-8.6	-8.5	-8.5
79.		Isoliquiritigenin	638278	-7.9	-7.8	-7.9	-7.9
80.		Naringetol	439246	-8.5	-8.4	-8.5	-8.5
81.		Pseudobaptigenin	5281805	-8.8	-8.9	-8.8	-8.8
82.		3,7,4'-Trihydroxyflavone	5281611	-8	-8	-8.1	-8
83.		Lupeol	259846	-7.6	-7.6	-7.7	-7.6
84.		Oleanolic acid	10494	-8.3	-8.3	-8.4	-8.3
85.	STAT3	Gallic acid	370	-4.2	-4.2	-4.2	-4.2
86.		Pterostilbene	5281727	-5.3	-5.3	-5.4	-5.3
87.		4-[2-Hydroxy-3-(4-hydroxyphenyl) propyl] phenol	185124	-4.8	-4.8	-4.9	-4.8
88.		Ebanol	6437266	-4.8	-4.8	-4.9	-4.8
89.		4-Hydroxybenzaldehyde	126	-4.2	-4.2	-4.1	-4.2
90.		beta-Eudesmol	91457	-5.3	-5.3	-5.4	-5.3
91.		Myristic acid	11005	-3.7	-3.8	-3.7	-3.7
92.		Palmitic acid	985	-4.1	-4.2	-4.1	-4.1
93.		Oleic acid	445639	-4.5	-4.4	-4.5	-4.5
94.		Linoleic acid	5280450	-4.9	-4.8	-4.9	-4.9
95.		Abscisic Acid	5280896	-5.3	-5.4	-5.3	-5.3
96.		Marsupsin	134369	-5.4	-5.5	-5.4	-5.4
97.		Epicatechin	72276	-5.8	-5.8	-5.8	-5.8
98.		Bergenin	66065	-5.8	-5.9	-5.8	-5.8
99.		liquiritigenin	114829	-5.8	-5.9	-5.8	-5.8
100.		Isoliquiritigenin	638278	-5.5	-5.4	-5.5	-5.5
101.		Naringetol	439246	-6.4	-6.3	-6.4	-6.4
102.		Pseudobaptigenin	5281805	-8.8	-8.7	-8.8	-8.8
103.		3,7,4'-Trihydroxyflavone	5281611	-6.2	-6.2	-8.4	-6.2
104.		Lupeol	259846	-6.8	-6.7	-8.4	-6.7
105.		Oleanolic acid	10494	-6.7	-6.6	-8.4	-6.6

Notes: T1-T3 represent three independent docking runs performed for each protein-ligand complex. The reported binding affinity corresponds to the representative (consensus) docking score used for subsequent analyses. Binding affinities are expressed in kcal/mol, with more negative values indicating stronger predicted binding.

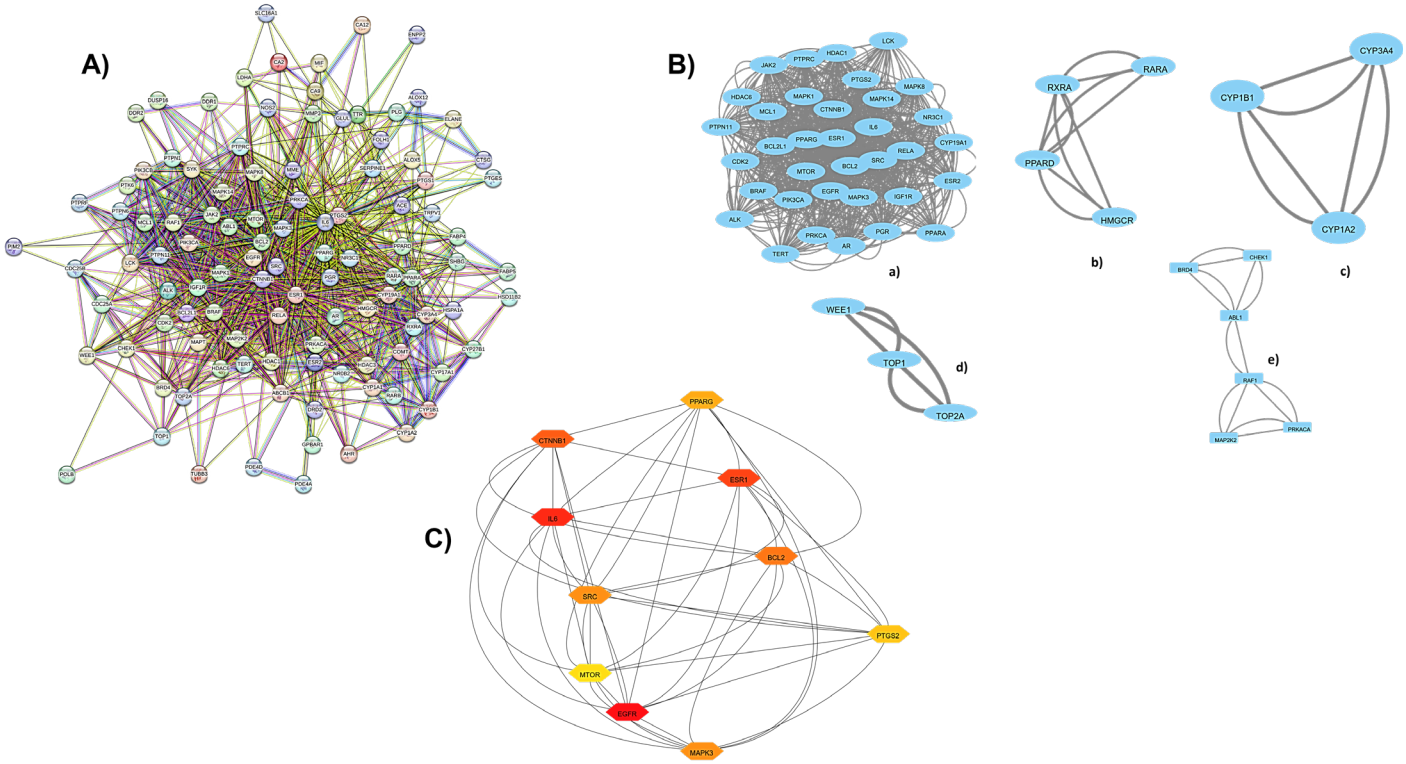


Figure 2: Protein-Protein Interaction (PPI) network architecture and topological analysis of HGSOC targets. (A) Global PPI network of 107 common targets generated via STRING. (B) MCODE-based cluster analysis identifying five functional modules: (a) Cluster 1, the primary regulatory core; (b-e) secondary metabolic and signalling clusters. (C) Topological hub-gene identification; nodes coloured red to yellow indicate increasing degree centrality, highlighting IL6, SRC, EGFR, and MTOR as master regulators.

in the previous revision). Pseudobaptigenin was therefore the only phytochemical to rank among the top two binders at all five targets, consistent with a genuine multitarget engagement profile across the hypoxia-glycolysis-survival axis rather than target-restricted binding.

Structural analysis of the highest-affinity complex, Pseudobaptigenin-FIH-1 (Figure 4B), showed the ligand occupying the co-crystallised-ligand-defined active site, engaging π-alkyl and π-π stacking with TRP296 and TYR102 and conventional hydrogen bonds with ARG238 and THR196 (14 total contacts; Table 3). 3,7,4′-Trihydroxyflavone (15 contacts) combined aromatic stacking with hydrogen bonding to ASP201 and GLN147, overlapping substantially with residues engaged by Pseudobaptigenin. Marsupsin formed the most extensive contact network observed (18 residues), including π-anion and π-cation interactions with ARG238. Naringetol engaged the regulatory loop adjacent to the catalytic pocket, liquiritigenin contacted the cleft via ILE281, and 4-[2-hydroxy-3-(4-hydroxyphenyl) propyl] phenol engaged the pocket through combined π-alkyl and hydrogen-bonding contacts (Table 3).

Validation of Molecular Docking by Redocking Analysis

Redocking validation was performed for the six lead ligand complexes at the FIH-1 (HIF1AN) active site and the top-ranked MTOR complex (Table 3). Four of the six FIH-1 complexes reproduced the reference binding pose within or at the conventional 2.0 Å RMSD threshold, including Pseudobaptigenin (1.8427 Å), marsupsin (1.9138 Å), 3,7,4′-trihydroxyflavone (1.9674 Å), and 4-[2-hydroxy-3-(4-hydroxyphenyl) propyl] phenol (1.9986 Å). Naringetol (2.1845 Å) and liquiritigenin (2.0739 Å) showed only marginal deviations from this threshold. The MTOR-Pseudobaptigenin complex also demonstrated reliable pose reproduction, with an RMSD of 1.7854 Å.

Although redocking was performed for all 105 ligand-target complexes as part of the docking workflow, RMSD values are reported only for the highest-affinity complexes (Table 3), which represent the principal candidates selected for further analysis. Overall, the RMSD results support the reproducibility of the predicted binding poses and the reliability of the docking protocol for identifying the lead phytochemical-target interactions evaluated in this study. Collectively, these RMSD-validated structural poses indicate that the lead phytochemicals occupy pharmacologically relevant, empirically defined positions within their respective targets, consistent with - though not proof of - a multitarget modulatory mechanism, pending the further experimental and validation work outlined in Section 4.2.

DISCUSSION

This is, to our knowledge, the first study to map a compound-target-disease network of *P. marsupium* phytochemicals against HGSOC. The 107 shared targets identified here provide a computational interface between traditional ethnopharmacological use and contemporary systems biology. The resulting PPI network was dense and centred on hub proteins including EGFR, IL6, ESR1, BCL2, and HIF1A (Szklarczyk *et al.*, 2023); the high connectivity of these nodes suggests that *P. marsupium* constituents, if pharmacologically active in this manner, would plausibly act on a coordinated regulatory core rather than a single pathway. This was reinforced by MCODE clustering, which resolved a central functional module integrating cell-cycle regulation, apoptosis, and metabolism processes mechanistically linked to HGSOC progression and chemoresistance (Franz *et al.*, 2023). On this basis, docking targets were selected to represent this axis at the structural level: FIH-1 (HIF1AN) a direct regulator of HIF-1α transactivation, was substituted here after post-hoc verification showed the originally intended HIF-1α structure to instead be FIH-1, together with PDK1, LDHA, MTOR, and STAT3, reflecting their combined role in the hypoxia-inflammation-metabolism axis. Molecular docking, validated by redocking/RMSD analysis, indicated favourable predicted binding affinities for lead phytochemicals, notably Pseudobaptigenin and marsupsin. These scores should be interpreted as comparative evidence within the present docking workflow; docking scores obtained using different structures and protocols are not directly quantitative measures of inhibitory potency. Pseudobaptigenin showed a predicted affinity of -9.7 kcal/mol for FIH-1; because FIH-1 is a negative regulator of HIF-1α, this finding should be interpreted as evidence of phytochemical interaction with the FIH-1 catalytic pocket rather than as evidence of direct HIF-1α suppression. PDK1 and LDHA active sites are consistent with the hypothesis that these compounds could interfere with the glycolytic (Warburg) phenotype characteristic of aggressive ovarian tumours (Atas *et al.*, 2020). These structural observations align with the enrichment analysis, which showed strong overrepresentation of HIF-1, PI3K-Akt, and ErbB signalling among the shared targets (Kanehisa *et al.*, 2025), together suggestive of coordinated engagement across the HIF-1-glycolysis-IL-6/STAT3 axis. By simultaneously engaging MTOR and downstream effectors (STAT3, LDHA), *P. marsupium* constituents could, in principle, help pre-empt compensatory feedback loops - such as mTORC2/AKT reactivation following glycolytic stress - that commonly underlie resistance to single-target inhibitors (Ghoneum *et al.*, 2020; Glaviano *et al.*, 2023); this remains a mechanistic hypothesis requiring functional confirmation, not an established effect.

Comparison with Previous Studies and Biological Plausibility

These findings are broadly consistent with, and extend, prior reports on individual *P. marsupium* constituents. Pterostilbene,

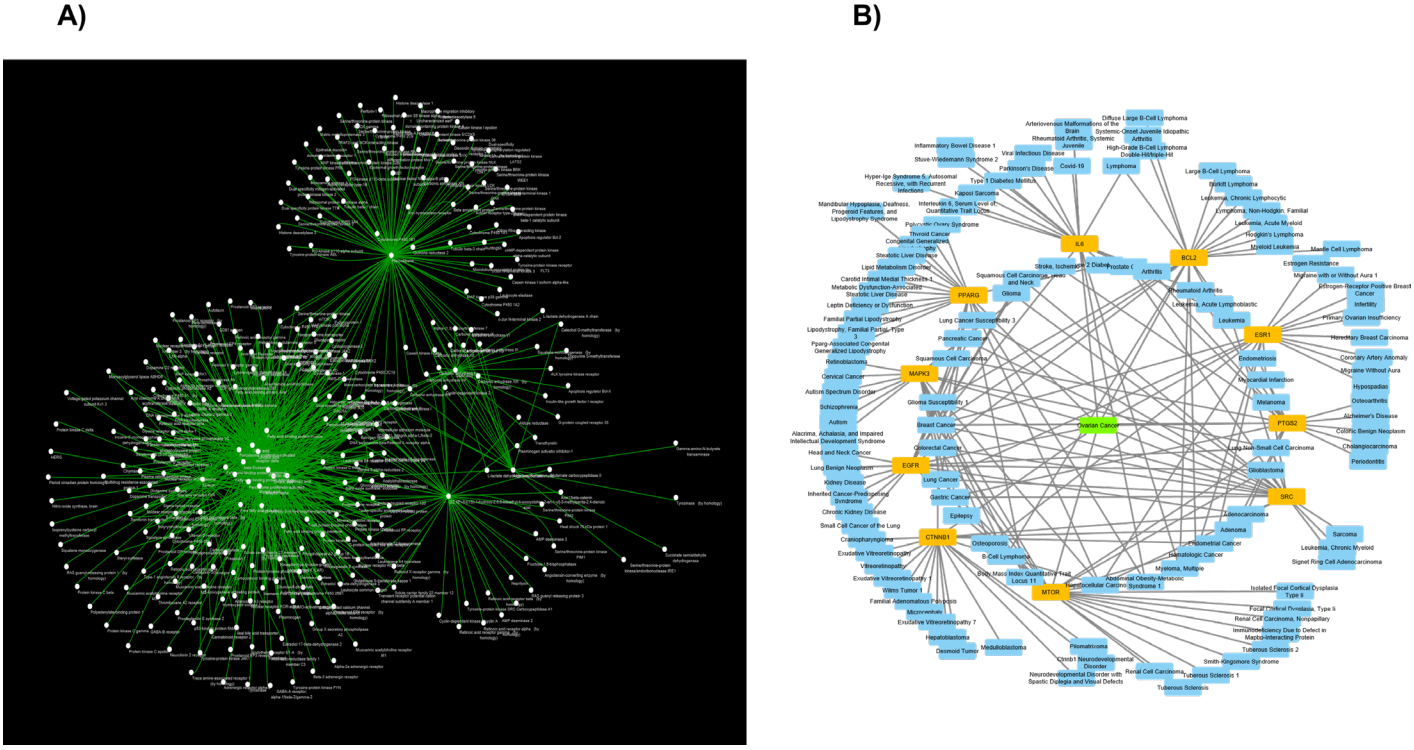


Figure 3: Multi-dimensional network pharmacology architecture of *P. marsupium* in HGSOC. (A) Drug-Target-Disease (D-T-D) network illustrating the regulatory influence of *P. marsupium* constituents across the proteome and disease landscape. (B) Integrated Target-Pathway-Disease network centred on hub genes (yellow nodes), depicting convergence of prioritised targets (MTOR, SRC, IL6, EGFR) onto oncogenic pathways and clinical manifestations of ovarian cancer (blue nodes).

Table 3: Protein-Ligand Interaction and Redocking/RMSD Validation Analysis (Lead Complexes).

Sl. No.	Receptors	Ligands	No of Interaction	Amino Acid Residues	RMSD (Å)
1.	FIH-1 (HIF1AN)	Pseudobaptigenin	14	LEU186, GLN147, TYR145, ARG238, GLN239, ASP201, TYR102, THR196, TRP296, HIS199, ILE281, LEU188, LYS214, PHE207	1.8427
2.	FIH-1 (HIF1AN)	3,7,4'-Trihydroxyflavone	15	LEU188, THR196, GLN147, LEU186, ARG238, GLN239, ASP201, TYR102, TRP296, HIS199, ILE281, HIS279, ILE273, PHE207, ASN205	1.9674
3.	FIH-1 (HIF1AN)	Marsupsin	18	LEU188, GLN147, THR196, LEU186, ASP201, ARG238, GLN239, TYR145, ILE281, PHE207, LYS214, HIS199, TRP296, ASN294, ASN205, TYR102, HIS279, ILE273	1.9138
4.	FIH-1 (HIF1AN)	Naringetol	6	ARG238, THR196, GLN147, ASP201, TYR102, ILE281.	2.1845
5.	FIH-1 (HIF1AN)	liquiritigenin	8	TYR102, ASP201, GLN239, THR196, GLN147, ILE281, LEU188, ASN205.	2.0739
6.	FIH-1 (HIF1AN)	4-[2-Hydroxy-3-(4-hydroxyphenyl) propyl] phenol	14	GLN147, THR196, LEU188, ILE281, ASP201, GLN239, TYR102, ARG238, PHE207, HIS199, TRP296, ASN205, ILE273, HIS279.	1.9986
7.	MTOR	Pseudobaptigenin	13	CYS2243, VAL2240, MET2345, TRP2239, LEU2185, GLY2238, LYS2187, TYR2225, ILE2356, ASP2195, ILE2237, ASP2357, GLU2190	1.7854

Notes: Atomic-level interaction data obtained from Discovery Studio Visualiser. RMSD calculated between the redocked and experimental co-crystallised ligand pose (heavy atoms), using the Superimpose Structures protocol in Discovery Studio Visualiser; conventionally, RMSD < 2.0 Å indicates successful pose reproduction.

the most extensively studied constituent of this plant, has previously been shown to modulate the MTA1/HIF-1α axis and suppress proliferation and angiogenesis in preclinical models of inflammatory and oncological disease (Liu *et al.*, 2024), supporting the biological plausibility, though not confirming the specific affinity values, of the HIF-1α-centred mechanism proposed here. Flavonoid-class phytochemicals structurally related to the present lead compounds (marsupsin, Naringetol, 3,7,4′-trihydroxyflavone, liquiritigenin) have separately been reported to modulate the PI3K/Akt/HIF-1α axis in therapy-resistant cancer cells (Mazurakova *et al.*, 2024), and STAT3 signalling has been independently characterised as a validated therapeutic vulnerability in ovarian cancer (Liang *et al.*, 2020), lending independent mechanistic support to the STAT3 docking findings reported here, which - following data verification - showed Pseudobaptigenin to be a comparably strong binder at STAT3 (-8.8 kcal/mol) to its affinities at the other four network-prioritised targets. Taken together, the present network pharmacology and docking evidence is consistent with, rather than definitively establishing, a multitarget hypoxia-inflammation-metabolism mechanism, and should be read as complementary to - not a replacement for - this existing experimental literature. Beyond molecular mechanics, these observations offer a plausible, though preliminary, scientific rationale for the traditional Ayurvedic use of *P. marsupium* in inflammatory and metabolic disease. The apparent polypharmacology arising from the plant's multiple constituents is compatible with a systems-level, rather than single-target, mode of action (Zhang *et al.*, 2013), consistent with the broader network pharmacology paradigm rather than direct clinical evidence of efficacy in HGSOC.

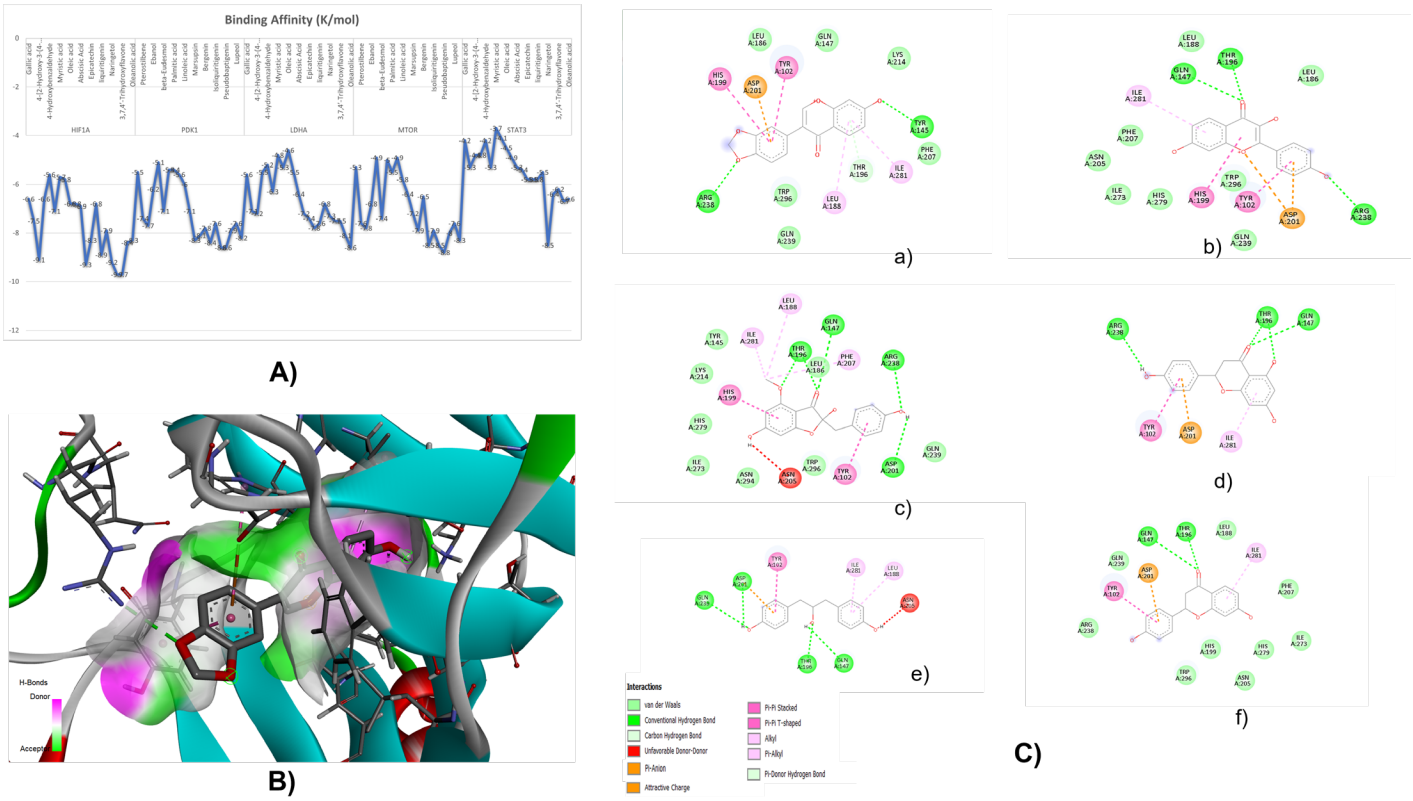


Figure 4: Molecular docking and atomistic interaction analysis of *P. marsupium* phytochemicals against HGSOC targets. (A) Comparative binding-affinity landscape (kcal/mol) of the bioactive library. (B) 3D representation of the FIH-1 (HIF1AN)-Pseudobaptigenin complex showing active-site occupancy (see Table 1 footnote and Section 2.7 for target identity note). (C) 2D ligand-residue interaction maps for lead candidates: (a) Pseudobaptigenin; (b) 3,7,4′-trihydroxyflavone; (c) marsupsin; (d) Naringetol; (e) liquiritigenin; (f) 4-[2-hydroxy-3-(4-hydroxyphenyl) propyl] phenol.

Study Limitations

This study is based entirely on computational analyses, providing a foundation for hypothesis generation and candidate prioritization. Although the docking protocol was supported by redocking and RMSD validation of the lead FIH-1 and MTOR complexes, future studies should extend validation to additional targets and incorporate molecular dynamics simulations to evaluate binding stability and receptor flexibility. The target prediction, network pharmacology, and ADMET analyses offer valuable preliminary insights but require experimental confirmation. Therefore, *in vitro* and *in vivo* studies are needed to validate the predicted molecular interactions, biological activities, and therapeutic potential of the identified phytochemicals in HGSOC.

CONCLUSION

This integrative network pharmacology and molecular docking study provides a computational rationale for further investigating *P. marsupium* as a potential multitarget agent against High-Grade Serous Ovarian Cancer (HGSOC). Twenty-one drug-like bioactive constituents were identified and docked in triplicate, among which Pseudobaptigenin, marsupsin, and Naringetol showed the most favourable and reproducible predicted binding profiles across the network-prioritised targets FIH-1 (HIF1AN), PDK1, LDHA, MTOR, and STAT3, with the lead poses supported by redocking/RMSD validation (Section 2.9). These findings offer a testable molecular hypothesis linking traditional Ayurvedic use of *P. marsupium* to a plausible mechanism of action against the HIF-1α-driven inflammation-metabolism axis implicated in HGSOC chemoresistance. As this is an entirely *in silico* study, these results should be regarded as preliminary and hypothesis-generating; experimental validation, including redocking/RMSD benchmarking of the remaining targets, molecular dynamics simulation, and *in vitro* and *in vivo* functional assays, is required before any conclusions can be drawn regarding the therapeutic or chemosensitising potential of these phytoconstituents in ovarian cancer.

ACKNOWLEDGEMENT

The authors thank the Saveetha Institute of Medical and Technical Sciences (SIMATS), Saveetha College of Pharmacy, for providing computational resources and research facilities.

ABBREVIATIONS

ADMET: Absorption, Distribution, Metabolism, Excretion, and Toxicity; **CXCL8:** C-X-C Motif Chemokine Ligand 8; **DAVID:** Database for Annotation, Visualization and Integrated Discovery; **FIH-1:** Factor Inhibiting HIF-1; **GO:** Gene Ontology; **HGSOC:** High-Grade Serous Ovarian Cancer; **HIF-1α:** Hypoxia-Inducible

Factor-1α; **IL-6:** Interleukin-6; **IMPPAT:** Indian Medicinal Plants, Phytochemistry and Therapeutics; **KEGG:** Kyoto Encyclopedia of Genes and Genomes; **LDHA:** Lactate Dehydrogenase A; **MCODE:** Molecular Complex Detection; **MTA1:** Metastasis-Associated Protein 1; **MTOR:** Mammalian Target of Rapamycin; **NF-κB:** Nuclear Factor Kappa B; **Nrf2:** Nuclear Factor Erythroid 2-Related Factor 2; **OMIM:** Online Mendelian Inheritance in Man; **PDB:** Protein Data Bank; **PDK1:** Pyruvate Dehydrogenase Kinase 1; **PPI:** Protein-Protein Interaction; **RMSD:** Root-Mean-Square Deviation; **STAT3:** Signal Transducer and Activator of Transcription 3; **TNF-α:** Tumor Necrosis Factor-Alpha; **VEGF:** Vascular Endothelial Growth Factor.

CONFLICT OF INTEREST

The authors declare that there is no conflict of interest.

ETHICS STATEMENT

This study is an entirely computational (*in silico*) investigation employing publicly available chemical, protein, and gene-annotation databases. No human participants, human biological samples, or animal subjects were involved at any stage of this work; accordingly, approval from an Institutional Ethics Committee or Institutional Animal Ethics Committee was not required, consistent with COPE and ICMJE guidance on ethics reporting for non-experimental, database-derived research.

DATA AVAILABILITY STATEMENT

All databases and software used (IMPPAT, PubChem, SwissADME, ProTox-3.0, SwissTargetPrediction, GeneCards, OMIM, STRING, Cytoscape, DAVID, CB-Dock, Discovery Studio Visualiser) are publicly or institutionally accessible as cited.

REFERENCES

Ahn, B., Moon, D., Kim, H., Lee, C., Cho, N. H., Choi, H., ... Park, E. (2024). Histopathologic image-based deep learning classifier for predicting platinum-based treatment responses in high-grade serous ovarian cancer. Nature Communications, 15(1), 4253. https://doi.org/10.1038/s41467-024-48667-6

Atas, E., Oberhuber, M., & Kenner, L. (2020). The implications of PDK1-4 on tumor energy metabolism, aggressiveness, and therapy resistance. Frontiers in Oncology, 10, 583217. https://doi.org/10.3389/fonc.2020.583217

Bader GD, Hogue CWV. (2003). An automated method for finding molecular complexes in large protein interaction networks. BMC Bioinformatics. 4(1), 2. https ://doi:10.1186/1471-2105-4-2

Banerjee, P., Eckert, A. O., Schrey, A. K., & Preissner, R. (2018). ProTox-II: a webserver for the prediction of toxicity of chemicals. Nucleic Acids Research, 46(W1), W257-W263. https://doi.org/10.1093/nar/gky318

Berman HM, Kleywegt GJ, Nakamura H, Markley JL. (2014). The Protein Data Bank archive as an open data resource. J Comput Aided Mol Des. 28(10), 1009-1014. https ://doi:10.1007/s10822-014-9770-y

Chin CH, Chen SH, Wu HH, Ho CW, Ko MT, Lin CY. (2014). cytoHubba: identifying hub objects and subnetworks from complex interactome. BMC Syst Biol. 8(Suppl 4), S11. https://doi:10.1186/1752-0509-8-S4-S11

Daina, A., Michielin, O., & Zoete, V. (2017). SwissADME: a free web tool to evaluate pharmacokinetics, drug-likeness and medicinal chemistry friendliness of small molecules. Scientific Reports, 7(1), 42717. https://doi.org/10.1038/srep42717

Daina, A., Michielin, O., & Zoete, V. (2019). SwissTargetPrediction: updated data and new features for efficient prediction of protein targets of small molecules. Nucleic Acids Research, 47(W1), W357-W364. https://doi.org/10.1093/nar/gkz382

Dassault Systèmes. (2016). Discovery Studio modelling environment (Release 4.x) [Computer software]. Dassault Systèmes.

Franz, M., Lopes, C. T., Fong, D., Kucera, M., Cheung, M., Siper, M. C., *et al*. (2023). Cytoscape.js 2023 update: A graph theory library for visualisation and analysis. Bioinformatics, 39, btad031. https://doi.org/10.1093/bioinformatics/btad031

Fu, R., Hu, R., Li, W., Lv, X., Zhao, H., & Li, F. (2025). Unveiling drug resistance pathways in high-grade serous ovarian cancer (HGSOC): Recent advances and future perspectives. Frontiers in Immunology, 16, 1556377. https://doi.org/10.3389/fimmu.2025.1556377

GeneCards®: the human gene database [Internet]. Rehovot: Weizmann Institute of Science; 2017 [cited 2025 Nov]. Available from: https://www.genecards.org

Ghoneum A, Abdulfattah AY, Said N. (2020) Targeting the PI3K/AKT/mTOR/NFκB axis in ovarian cancer. J Cell Immunol. 2(2), 68-73. https://doi:10.33696/immunology.1.022

Ghoneum A, Gonzalez D, Afify H, Shu J, Hegarty A, Adisa J, *et al.* (2022). Compound C inhibits ovarian cancer progression via PI3K-AKT-mTOR-NFκB pathway. Cancers. 14(20), 5099. https://doi:10.3390/cancers14205099

Glaviano A, Foo ASC, Lam HY, Yap KCH, Jacot W, Jones RH, *et al.* (2023). PI3K/AKT/mTOR signal transduction pathway and targeted therapies in cancer. Mol Cancer. 22(1), 138. https://doi:10.1186/s12943-023-01827-6

Hamosh, A., Scott, A. F., Amberger, J. S., Bocchini, C. A., & McKusick, V. A. (2005). Online Mendelian Inheritance in Man (OMIM), a knowledgebase of human genes and genetic disorders. Nucleic Acids Research, 33, D514–D517. https://doi.org/10.1093/nar/gki033

Kanehisa M, Furumichi M, Sato Y, Matsuura Y, Ishiguro-Watanabe M. (2025) KEGG: biological systems database as a model of the real world. Nucleic Acids Res. 53(D1), D672-D677. https://doi:10.1093/nar/gkae909

Kanehisa M, Goto S. (2000). KEGG: Kyoto Encyclopedia of Genes and Genomes. Nucleic Acids Res. 28(1), 27-30. https://doi:10.1093/nar/28.1.27

Kanehisa, M. (2000). Post-genome informatics. Oxford University Press. https://doi.org/10.1093/oso/9780198503279.001.0001

Kim, S., Chen, J., Cheng, T., Gindulyte, A., *et al.* (2022). PubChem 2023 update. Nucleic Acids Research, 51(D1), D1373-D1380. https://doi.org/10.1093/nar/gkac956

Lando D, Peet DJ, Whelan DA, Gorman JJ, Whitelaw ML. (2002) Asparagine hydroxylation of the HIF transactivation domain: a hypoxic switch. Science. 295(5556), 858-861. https://doi:10.1126/science.1068592

Laskowski RA, Jabłońska J, Pravda L, Vařeková RS, Thornton JM. (2018). PDBsum: structural summaries of PDB entries. Protein Sci. 27(1), 129-134. https://doi:10.1002/pro.3289

Liang R, Chen X, Chen L, Wan F, Chen K, Sun Y, Zhu X. (2020). STAT3 signalling in ovarian cancer: a potential therapeutic target. J Cancer. 11(4), 837-848. https://doi:10.7150/jca.35011

Lipinski CA, Lombardo F, Dominy BW, Feeney PJ. (2001). Experimental and computational approaches to estimate solubility and permeability in drug discovery and development settings. Advanced Drug Delivery Reviews. 46(1-3), 3-26. doi:10.1016/S0169-409X(00)00129-0.

Liu Y, Yang X, Gan J, Chen S, Xiao ZX, Cao Y. (2022)., CB-Dock2: improved protein-ligand blind docking by integrating cavity detection, docking and homologous template fitting. Nucleic Acids Res. 50(W1), W159-W164. https://doi:10.1093/nar/gkac394

Liu, P., Tang, W., Xiang, K., & Li, G. (2024). Pterostilbene in the treatment of inflammatory and oncological diseases. Frontiers in Pharmacology, 14, 1323377. https://doi.org/10.3389/fphar.2023.1323377

Mazurakova, A., Koklesova, L., Hurta Csizmár, S., Samec, M., Brockmueller, A., Šudomová, M., Biringer, K., Kudela, E., Pec, M., Mathews Samuel, S., Kassayova, M., Hassan, S. T. S., Smejkal, K., Shakibaei, M., Büsselberg, D., Saso, L., Kubatka, P., & Golubnitschaja, O. (2024). Significance of flavonoids targeting PI3K/Akt/HIF-1α signaling pathway in therapy-resistant cancer cells: A potential contribution to the predictive, preventive, and personalized medicine. Journal of Advanced Research, 55, 103–118. https://doi.org/10.1016/j.jare.2023.02.015

Oliveros, J. C. (2007). Venny: An interactive tool for comparing lists with Venn's diagrams. Bioinformatics Research Group, Centro Nacional de Biotecnología. https://bioinfogp.cnb.csic.es/tools/venny/index.html

Opara, J. K., Sanchez, S., Thomas, S. M., & Anant, S. (2025). Natural products targeting cancer stem cells: A promising therapeutic approach. Exploration of Drug Science, 3. https://doi.org/10.37349/eds.2025.1008106

Qin, J., Liu, Y., Lu, Y., Liu, M., Li, M., Li, J., & Wu, L. (2017). Hypoxia-inducible factor 1 alpha promotes cancer stem cells-like properties in human ovarian cancer cells by upregulating SIRT1 expression. Scientific Reports, 7(1), 10592. https://doi.org/10.1038/s41598-017-09244-8

Rahman, M. A., Jalouli, M., Bhajan, S. K., Al-Zharani, M., & Harrath, A. H. (2025). The role of Hypoxia-Inducible Factor-1A (HIF-1A) in the progression of ovarian cancer: Perspectives on Female Infertility. Cells, 14(6), 437. https://doi.org/10.3390/cells14060437

Rappaport N, Twik M, Plaschkes I, Nudel R, Stein TI, Levitt J, *et al.* (2017). MalaCards: an amalgamated human disease compendium with diverse clinical and genetic annotation and structured search. Nucleic Acids Res. 45(D1), D877-D887. https://doi:10.1093/nar/gkw1012

Shaikat, A. H., Azad, S. a. K., Tamim, M. a. R., Ullah, M. S., *et al.* (2025). Investigating hypoxia-inducible factor signaling in cancer: Mechanisms, clinical implications,

targeted therapeutic strategies, and resistance. Cancer Pathogenesis and Therapy, 4(3), 174-191. https://doi.org/10.1016/j.cpt.2025.07.003

Sherman BT, Panzade G, Imamichi T, Chang W. (2024). DAVID Orthologue: an integrative tool to enhance functional analysis through orthologs. Bioinformatics. 40(10), btae615. https://doi:10.1093/bioinformatics/btae615

Szklarczyk D, Kirsch R, Koutrouli M, Nastou K, Mehryary F, Hachilif R, *et al.* (2023). The STRING database in 2023: protein-protein association networks and functional enrichment analyses for any sequenced genome of interest. Nucleic Acids Res. 51(D1), D638-D646. https://doi:10.1093/nar/gkac1000

Vivek-Ananth, R., Mohanraj, K., Sahoo, A. K., & Samal, A. (2023). IMPPAT 2.0: An Enhanced and Expanded Phytochemical Atlas of Indian Medicinal plants. ACS Omega, 8(9), 8827-8845. https://doi.org/10.1021/acsomega.3c00156

Wagner, V., Morton, M., Dorayappan, K. D. P., Gonzalez, A., *et al.* (2025). Circulating extracellular vesicles protein expression for early prediction of platinum-resistance in high-grade serous ovarian cancer. Oncogene, 44(17), 1197-1203. https://doi.org/10.1038/s41388-025-03382-4

Wang, X., Du, Z.-W., Xu, T.-M., Wang, X.-J., Li, W., Gao, J.-L., Li, J., & Zhu, H. (2021). HIF-1α is a rational target for future ovarian cancer therapies. Frontiers in Oncology, 11, 785111. https://doi.org/10.3389/fonc.2021.785111

Warrier, P. K., Nambiar, V. P. K., Ramankutty, C., & Nair, R. V. (1994). Indian medicinal plants: A compendium of 500 species. Orient Longman

Zhang, G., Li, Q., Chen, Q., & Su, S. (2013). Network Pharmacology: a new approach for Chinese herbal medicine research. Evidence-based Complementary and Alternative Medicine, 2013(1), 1-9. https://doi.org/10.1155/2013/621423

Cite this article: Gopinath S, Balakrishnan P, Muli Y, Sirajudeen S, Rajathi PVK, Vijayan MR. Integrative Network Pharmacology and Molecular Docking Reveal the Multitarget Anti-HGSOC Potential of *Pterocarpus marsupium* Phytoconstituents via Modulation of HIF-1α-Driven Inflammation-Metabolism Crosstalk. J Young Pharm. 2026;18(3):917-30.